RAA 2018 Vol. **18** No. **12**, 147(14pp) doi: 10.1088/1674–4527/18/12/147

http://www.raa-journal.org *http://iopscience.iop.org/raa*

***R**esearch in*
***A**stronomy and*
***A**strophysics*

The SAGE photometric survey: technical description

Jie Zheng[1,2], Gang Zhao[1,2], Wei Wang[1,3], Zhou Fan[1], Ke-Feng Tan[1], Chun Li[1] and Fang Zuo[1]

[1] Key Laboratory of Optical Astronomy, National Astronomical Observatories, Chinese Academy of Sciences, Beijing 100101, China; *gzhao@nao.cas.cn*
[2] School of Astronomy and Space Science, University of Chinese Academy of Sciences, Beijing 100049, China
[3] Chinese Academy of Sciences South America Center for Astronomy, China-Chile Joint Center for Astronomy, National Astronomical Observatories, Chinese Academy of Sciences, Beijing 100101, China

Received 2018 April 29; accepted 2018 May 25

Abstract To investigate a huge sample of data related to the Stellar Abundance and Galactic Evolution (SAGE) survey in more detail, we are performing a northern sky photometric survey named SAGES with the SAGE photometric system. This system consists of eight filters: Strömgren-u, SAGE-v, SDSS g, r, i, DDO-51, H$\alpha_{\rm wide}$ and H$\alpha_{\rm narrow}$, including three Sloan broadband filters, three intermediate-band filters, two narrow-band filters and one newly-designed narrow-band filter. SAGES covers ∼12 000 square degrees of the northern sky with $\delta > -5^\circ$, excluding the Galactic disk ($|b| < 10^\circ$) and the sky area 12 h <RA <18 h. The photometric detection limit depth at signal-to-noise ratio 5σ can be as deep as V∼20 mag. SAGES will produce a photometric catalog with uniform depth for ∼500 million stars with atmospheric parameters including effective temperature $T_{\rm eff}$, surface gravity $\log g$ and metallicity [Fe/H], as well as interstellar extinction to each individual target. In this work, we will briefly introduce the SAGE photometric system, the SAGE survey and a preliminary test field of the open cluster NGC 6791 and its surroundings.

Key words: methods: observational — techniques: photometric — surveys — astrometry — catalogs

1 INTRODUCTION

Astronomy is a basic science that strongly relies on the development of observations, and sky surveys of large areas are among the most important ladders for progress in astronomy. In recent decades, the Sloan Digital Sky Survey (SDSS, York et al. 2000), Two Micron All Sky Survey (2MASS, Skrutskie et al. 2006) and other sky surveys have demonstrated that such data are very important, leading to numerous newly-identified objects, newly-studied events and new physics, and some have even opened new areas of modern astronomy. Besides photometric sky surveys, spectral surveys are also fruitful, for example LAMOST (Zhao et al. 2012) has provided the largest spectral data set thus far and plays an important role in finding metal-poor stars (Li et al. 2015a), high- or hyper-velocity stars (Li et al. 2015b), white dwarfs (Zhao et al. 2013) and emission line objects (Shi et al. 2014).

As far as we know, the Geneva-Copenhagen Survey (GCS, Nordström et al. 2004) is the only sky survey based on the Strömgren-Crawford (SC) system (Strömgren 1963, 1964; Crawford et al. 1970), which includes intermediate and narrow band filters, dedicated to stellar atmospheric parameters. The GCS survey is volume complete to a distance of 40 pc down to $V\sim 8.5$ mag. The HM catalog (Hauck & Mermilliod 1998) collected all measurements in these systems, which include only ∼66 000 stars in total. This situation is mainly due to the fact that the narrow and medium bans require much more integration time, especially the Strömgren-u and H$\beta_{\rm n}$-bands, than broadband filters, to achieve a similar brightness limit. With the development of CCD photometry, much better sensitivity in the blue range of CCD detectors and the emergence of tens of 4–10 m telescopes, now is the best opportunity to conduct a sky survey with a number of infrequently-used smaller aperture telescopes with wide-field cameras in narrow and

medium bandpasses which are dedicated to the determination of the atmospheric parameters of stars much fainter than what are available in GCS.

However, among all the previous or currently ongoing sky surveys, few of them are specifically focused on stellar atmospheric parameters. Under this situation, we are performing a deep photometric sky survey using a combination of narrow, intermediate and broadband filters, with the main purpose to determine stellar parameters for hundreds of millions of stars with accuracies significantly better than those obtained with broadband filters and comparable to those determined spectroscopically. We will introduce the design of our sky survey and observations, the data reduction pipeline and the performance of our test field.

2 THE SAGE PHOTOMETRIC SURVEY AND RELATED OBSERVATIONS

2.1 The SAGE Photometric System

The Johnson UBV photometric system (Johnson & Morgan 1953) is one of the earliest and most widely used among all standard photoelectric photometric systems. The revolutionary project SDSS, by providing an unprecedented database of photometric observations of stars and galaxies, has essentially made its bandpasses, the SDSS photometric system, $u'g'r'i'z'$ (Fukugita et al. 1996), the current standard for most (if not all) ongoing and future photometric surveys and most photometric imaging. However, it is unfortunate that SDSS filters were chosen basically to determine photometric redshifts for galaxies, rather than to isolate relevant stellar absorption features in particular bands, and therefore this system is not ideal for accurate determinations of the metallicities and gravities of stars.

Thanks to narrower bandpasses and specific definition of the u band, the SC system provides a reliable method to determine stellar parameters for stars with a wide range of spectral types (e.g., early or late type stars, and metal-poor stars). In particular, this photometric system, composed of the Strömgren $ubvy$ plus the Hβ wide and narrow bandpasses, can accurately identify stars at various evolutionary stages (Strömgren 1963; Árnadóttir et al. 2010). Several indices, including $m1 = (v-b)-(b-y)$, $c1 = (u-v)-(v-b)$ and $\beta = \beta_{\rm n} - \beta_{\rm w}$, can be used to measure metallicity, surface gravity and strength of the Hβ line without being affected by extinction.

In order to obtain accurate stellar atmosphere parameters with high efficiency, we constructed a new photometric system: the SAGE system, by combining multiple photometric systems and adding several new filters. This system consists of eight filters: Strömgren-u, SAGE-v, SDSS g, r, i, DDO-51, H$\alpha_{\rm wide}$ and H$\alpha_{\rm narrow}$ (hereafter $u_{\rm SC}$, $v_{\rm SAGE}$, g, r, i, DDO51, H$\alpha_{\rm w}$ and H$\alpha_{\rm n}$, respectively). Their effective wavelengths and bandwidths are shown in Table 1 and their normalized transmission curves are plotted in Figure 1. All magnitudes of the SAGE system are expressed in the AB system.

The SAGE system can effectively determine stellar atmospheric parameters, including effective temperature $T_{\rm eff}$, surface gravity $\log g$ and metallicity [Fe/H], as well as extinction. These parameters can be determined by $(g-i)$, $(u_{\rm SC}-v_{\rm SAGE})$, $(v_{\rm SAGE}-g)$ and $({\rm H}\alpha_{\rm n}-{\rm H}\alpha_{\rm w})$ in the system. The response curves of the $u_{\rm SC}$ and $v_{\rm SAGE}$ filters are located on both sides of the Balmer jump and can be used to measure its intensities. Moreover, there is almost no overlapping area between the two filters of the SAGE system, and more accurate $\log g$ measurement results can be obtained. We prefer our $v_{\rm SAGE}$ rather than Strömgren-v as it is bluer by $\sim$150 Å, aiming to include Ca II H & K doublets for better correlation with stellar metallicities. The SDSS g and r filters should have similar usages as Strömgren b and y, but they will consume significantly less observation time with the latter two. We change the Hβ filters to Hα ones as the CCD efficiency is similar at both wavelengths, but the latter ones have higher sensitivity to stellar or nebular spectra. In G- and K-type stars, Hβ lines are weaker than Hα ones, so measurement of these lines will be more efficient. The DDO51 filter is employed to further constrain stellar gravity. For more details, please refer to Fan et al. (2018).

2.2 The SAGE Photometric Survey

The SAGE Photometric Survey (SAGES) is a northern sky survey with the SAGE photometric system covering about 12 000 square degrees. This survey was firstly proposed in 2014 (Wang et al. 2014) to be conducted with the full SC system. After further investigations, we believe our SAGE system is superior to the SC system and the SAGE system is therefore adopted in our survey instead of the SC system. The SAGES project started in 2015, and the plan is to finish observations, flux calibrations and astrometric calibrations in 4 to 5 years. We aim to achieve a survey depth to 20 mag with a signal-to-noise ratio (SNR) of 5:1 in the Johnson V

Table 1 The SAGE Photometric System

Band	$u_{\rm SC}$	$v_{\rm SAGE}$	g	r	i	DDO51	H$\alpha_{\rm n}$	H$\alpha_{\rm w}$
Effective wavelength (Å)	3520	3950	4639	6122	7439	5132	6563	6563
Bandwidth (Å)	314	290	1280	1150	1230	162	29	136

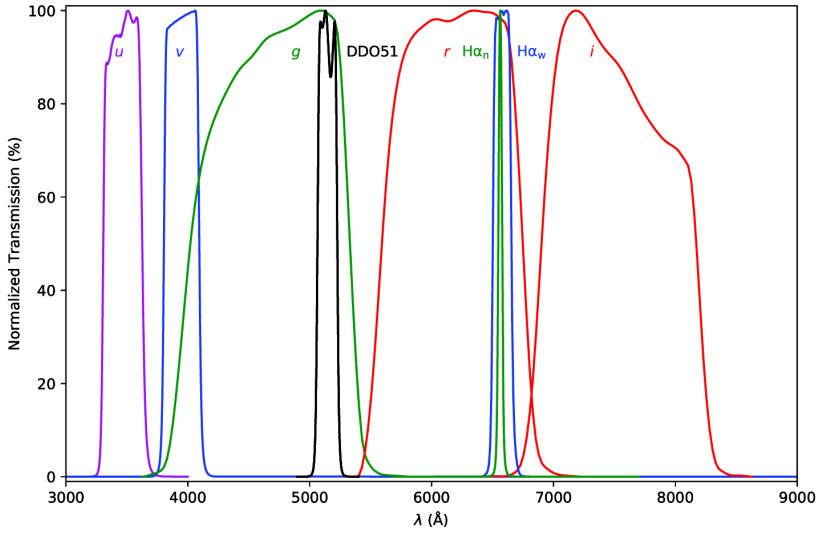

Fig. 1 Normalized transmission curves of the SAGE filters.

band on the Vega system, which corresponds to depths of ∼21.5 in $u_{\rm SC}$, ∼21.0 in $v_{\rm SAGE}$ and ∼19.5 in g, r and i. Note that these are magnitudes expressed in the AB system, and all fluxes and errors are measured from point sources extracted by Source Extractor (SExtractor, Bertin & Arnouts 1996) with aperture photometry with an aperture diameter of 2.5 times the mean full width at half maximum (FWHM) of objects in each image. SAGES will produce a photometric catalog with uniform depth for ∼500 million stars with atmospheric parameters including effective temperature $T_{\rm eff}$, surface gravity $\log g$ and metallicity [Fe/H], as well as extinction to each individual target. Value-added information like stellar radius may be provided as well when combined with high precision parallax measurements by the *Gaia* mission (Gaia Collaboration et al. 2018).

Completing an entire northern sky survey with non-broadband filters takes a lot of telescope time even with wide-field cameras. Therefore, we decided to use three telescopes almost simultaneously to conduct the survey in different bandpasses, as described below. We note that with careful design of standard star observations, the absolute flux calibration is expected to be as good as 0.02 mag and the uniformity should be better than 0.02 mag in our first data release. We expect these values to be improved in later data releases.

2.3 Telescopes and Instruments

Given that the $u_{\rm SC}$-band has a wavelength coverage very close to the atmospheric cutoff, plus the fact that in this band typical stars are intrinsically very faint, we must analyze integration time in $u_{\rm SC}$ to achieve our proposed 5σ-limit of 21.5 mag. Considering that we would like to keep the observations in three different telescopes at the same pace, and the fact the Bok 90-inch telescope[1] has an aperture twice as large as the other two, we decided to conduct the observations in $u_{\rm SC}$ and $v_{\rm SAGE}$. The Bok telescope is an equatorially mounted telescope located at Kitt Peak, which is at $30°57'46.5''$N by $111°36'01.6''$W, and 2071 meters above sea level. The Bok Telescope is administered by Steward Observatory, which is part of the University of Arizona.

The instrument named 90Prime consists of four $4{\rm k} \times 4{\rm k}$ back-illumination CCDs and is installed at the prime focus of the telescope. The field of view is around

[1] *http://james.as.arizona.edu/∼psmith/90inch/90inch.html*

$1.08^\circ \times 1.03^\circ$ with gaps of $\sim 166''$ in right ascension (RA) and $\sim 54''$ in declination (Dec) between the CCDs.

Figure 2 shows the layout of 90Prime. We choose the slow mode to read the whole frame of 90Prime, which takes about 37 s with a noise level of 6–10 electrons per pixel. We perform $u_{\rm SC}$- and $v_{\rm SAGE}$-band observations using the Bok telescope.

For the SDSS g, r and i-bands, we decided to use the Nanshan One-meter Wide-field Telescope (hereafter NOWT) to carry out observations. NOWT is an altazimuth-mounted telescope located at Nanshan Station, which is at $43°16'45.0''$N by $87°10'38.3''$E, and 2081 meters above sea level. NOWT is administered by Xinjiang Astronomical Observatory (XAO), Chinese Academic of Sciences (CAS). A wide field camera, consisting of a $4\rm k \times 4\rm k$ blue-enhanced back-illuminated CCD, is installed at the prime focus of NOWT, with a field of view of about $1.5^\circ \times 1.5^\circ$. The typical readout speed is about 40 s via four parallel amplifiers with a readout noise of 8–10 electrons (Liu et al. 2014). As the SDSS survey has covered ∼9000 square degrees in the northern sky, we only need to conduct the observations in gri-bands for the other ∼4000 square degrees, including some overlapping regions, to secure flux calibrations.

The Zeiss-1000 Telescope at the Maidanak Astronomical Observatory (MAO), Ulugh Beg Astronomical Institute, Uzbek Academy of Sciences (Ehgamberdiev et al. 2000) is being upgraded. It is expected to be available in late 2018. Its current field of view is $32.9' \times 32.9'$. We will perform $\rm H\alpha_w$ and $\rm H\alpha_n$ observations there.

2.4 Observations and Progress

SAGES is proposed to cover the northern sky with $\delta > -5^\circ$, excluding the bright, high extinction Galactic disk ($|b| < 10^\circ$). Meanwhile, because of the time allocation of Bok, we exclude the sky area of 12 h <RA < 18 h from the current observation, but may target it in future projects. Figure 3 demonstrates the proposed coverage of SAGES.

For all the observations with the three telescopes, we have the same strategy where the only differences are filters and exposure times. On clear nights, the exposure time for each band is listed in Table 2. The exposure times will increase as the airmass increases. They will also increase with the amount of clouds. For each night we make a plan based on the previous footprint and the current date, so that most fields are observed at the lowest possible airmass and the time for telescopes to slew is the shortest. Normally, a field will be observed only once for each band.

Table 2 Exposure Time for Each Band during Clear Nights

Band	$u_{\rm SC}$	$v_{\rm SAGE}$	g	r	i
Exposure time (s)	60	20	30	40	40

To achieve reliable and consistent flux and astrometric calibrations, we leave sufficient overlapping regions between adjacent fields. The observation fields at the same declination form a horizontal stripe, and in a given stripe an overlap of ∼20% is reserved between adjacent fields in the same stripe. Meanwhile an overlap of ∼20% is set between adjacent stripes. As a result, each field will have one neighbor in the east and one in the west with ∼20% of the area being an overlapping region in each direction. It has two northern and two southern neighbors with overlapping fractions of 0%–20% for each field-to-field pair, but in total 20% for each direction.

Figure 4 shows the overlap between Bok Field 6352 and its neighbors as an example, and the distributions are very similar with different field scales due to different sizes of the fields-of-view for the other two telescopes. We note that Figure 4 does not show the internal gaps between mosaic CCDs of Bok.

We estimate that ∼36% of the survey area will be visited only once, 32%–48% of the survey area will be visited twice, ∼24% to be visited three times and the remaining small fraction of <16% to be visited four times. The time span between visits could range from minutes to days to years. With multiple visits for a total of 36% of our survey area, on one hand, reliable flux and astrometric calibrations could in principle be achieved, and on the other hand, time-domain alerts should be able to be generated for follow-up studies.

SAGES began its observations in the autumn of 2015. By the end of Jan 2018, observations of g, r and i at NOWT were completed, meanwhile, observation of $u_{\rm SC}$ and $v_{\rm SAGE}$ on Bok are about 2/3 completed and the remaining 1/3 is expected to be done in 2019. Observations to be done at MAO are scheduled for late 2018. The current progress on the survey as of January 2018 is listed in Table 3, and the up-to-date progress can be found at the official website for SAGES[2].

[2] *http://sage.bao.ac.cn/surveyobs/obsfootprint.php*

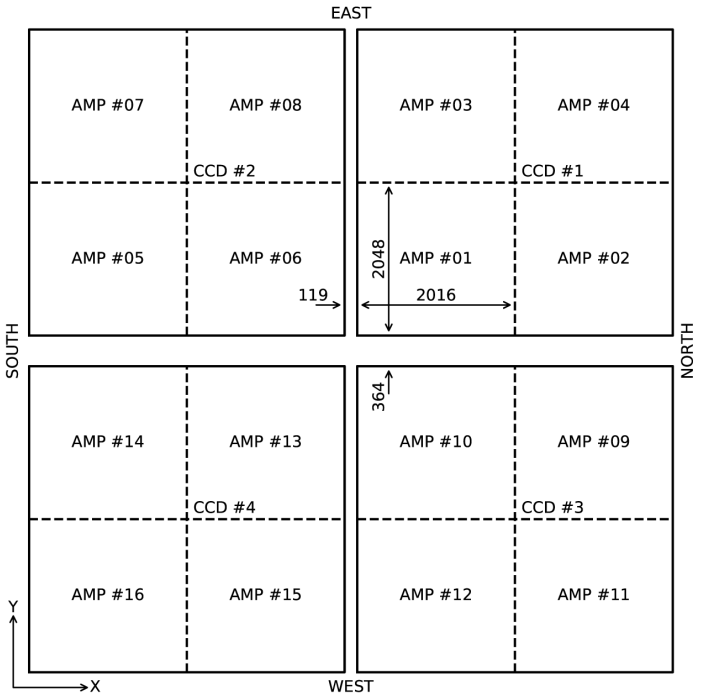

Fig. 2 Layout of the 90Prime detector array (not to scale, expressed in pixels).

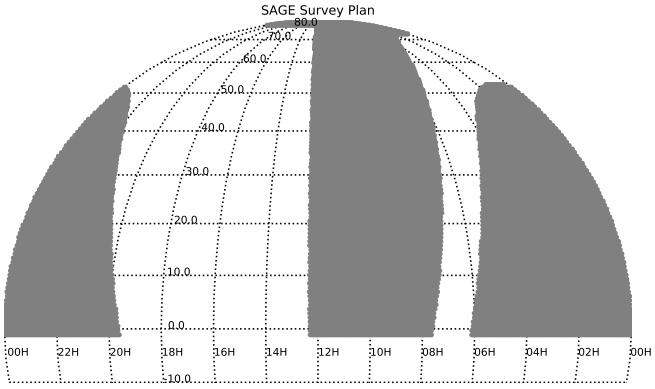

Fig. 3 Coverage plan for the SAGE photometric survey.

Table 3 The Observation Progress of SAGES as of January 2018.

Band	$u_{\rm SC}$	$v_{\rm SAGE}$	g	r	i
Field number	12364	11376	4254	4254	4254
Area covered (deg^2)	7913	7280	4254	4254	4254
Percent (%)	69.7	64.2	100.0	100.0	100.0

3 THE DATA REDUCTION PIPELINE

We have developed a data reduction pipeline to semi-automatically perform standard reduction procedures including bias subtraction, flat-fielding, distortion correction, astrometry and aperture photometry. We will introduce our pipeline briefly in this section, as shown in Figure 5.

3.1 Correction of Images

The ultimate purpose of image reduction is to convert detector digital counts given in raw CCD images to electron count rates (e^- s^{-1}), through a series of procedures including overscan and bias correction, flat-fielding and crosstalk removal.

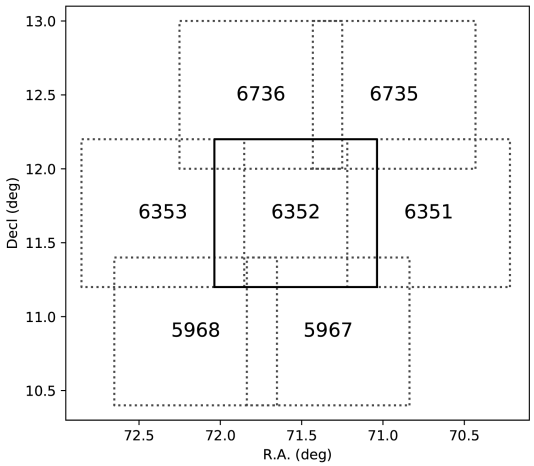

Fig. 4 Overlap between survey fields.

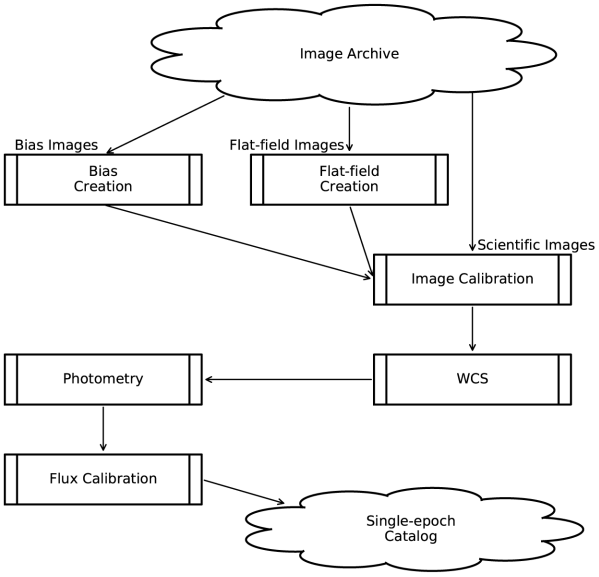

Fig. 5 A flowchart depicting the science data pipeline.

The pipeline computes the median value of each row in the overscan area, then subtracts it from the corresponding rows in the image. Following the technique performed in Zou et al. (2017) for BASS data, which were obtained also with 90Prime, a Gaussian smoothing is applied to the count variations in the row direction, which is believed to better represent the bias level along the row direction. A section of the overscan data and its smoothed result is displayed in Figure 6. For all images, including bias, flat-field and science images, overscan correction is the first step in data reduction. We use the same method to correct overscan at both Bok and NOWT after tests.

Before and after each night of observations, a set of 10 bias exposures is taken. A master bias frame can be easily constructed, with each pixel's value being the median value of the 20 exposures with the same pixels. With this master bias image, all science exposures and flat-field exposures taken on the same night can be bias-subtracted accordingly.

The next step is to perform flat-fielding for science exposures with flat-field exposures taken of the sky during twilight, or those taken on a curtain illuminated uniformly by a scanning lamp during the daytime, or super night-sky flat by merging all the science images taken

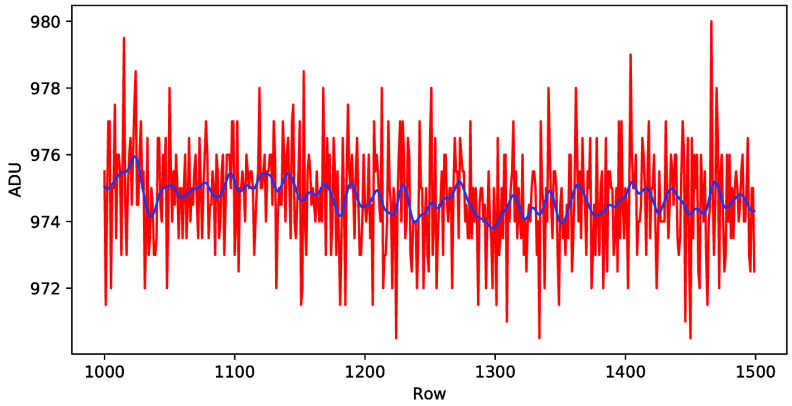

Fig. 6 ADU of overscan region (*red*) and a smoothed curve (*blue*).

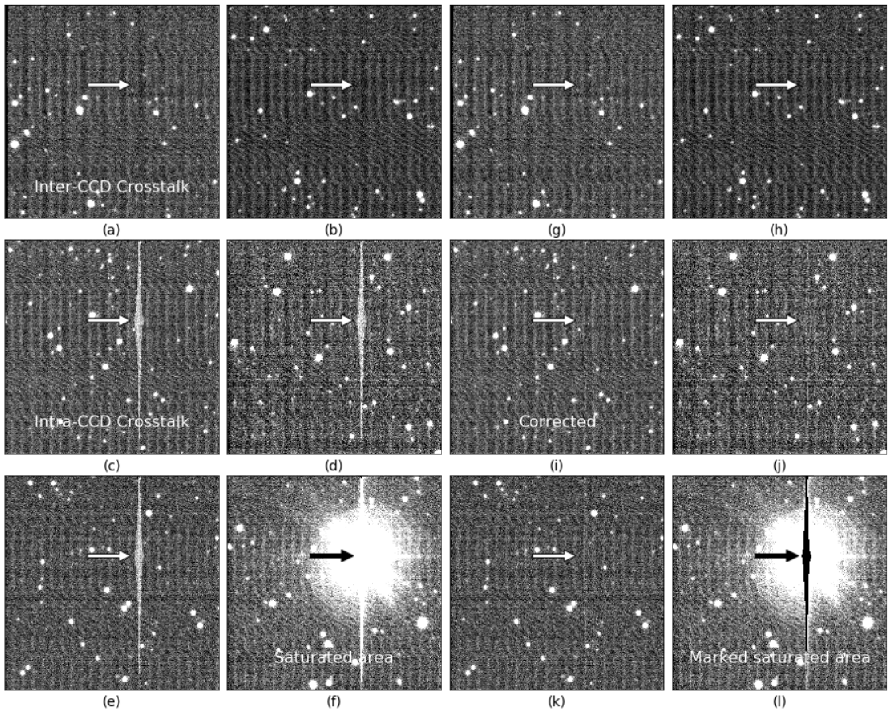

Fig. 7 A typical example of crosstalk and the image after correction in inverted gray scale. Panels (a–f) are original images. Panel (f) is the source, panels (c–e) are polluted by intra-CCD crosstalk and panels (a–b) are polluted by inter-CCD crosstalk. Panels (g–k) are corrected images of (a–e), respectively. In panel (j), the saturated area is marked. In all panels, the polluted and corrected areas are pointed out. Stripes caused by interference from the camera controllers, appearing as large-scale patterns, can be seen in images. We are working on this and they will be removed in the future.

over the course of a night. As usual, the priority is to use high SNR twilight flats to correct the large-scale illumination trend and employ the dome flats to correct for pixel-to-pixel variations when applicable, and if not, a super night-sky flat will be used instead. We estimate that our master flat images will be accurate to 1 percent for most nights.

The 90Prime consists of four CCDs and each has four amplifiers for parallel readout. This function of multi-channel CCD readout can significantly reduce the time spent on reading the detector. The disadvantage of this option is the so-called amplifier crosstalk, which causes contamination across the output amplifiers, typically at the level of 1:10 000. This can be a serious prob-

lem for high precision photometry and when bright stars saturate CCD detectors.

We follow the method suggested by Freyhammer et al. (2001) to remove crosstalk. We compute the crosstalk coefficient from bright sources detected and their crosstalk signal on other amplifiers used in acquiring the image. We use a large number of images to estimate the crosstalk coefficients between amplifiers. The pipeline computes the crosstalk pollution from bright areas with the coefficients, then applies it to correct the image. The overall ratio of crosstalk is about $5:10\,000$ for 90prime, while inter-CCD crosstalk ratios are greater and intra-CCD ratios are lower.

Figure 7 shows a typical crosstalk and the image after correction. Panels (a–f) are original images. Panel (f) is the source, panels (c–e) are polluted by intra-CCD crosstalk and panels (a–b) are polluted by inter-CCD crosstalk. Panels (g–k) are corrected images of (a-e), respectively. In panel (j), the saturated area is marked. In all panels, the polluted and corrected areas are pointed out.

In Figure 7, stripes caused by interference from the camera controllers can be seen. They are large-scale patterns but not uniform and do not fully cover the whole image. We are working on this issue and they will be removed in a future version of the pipeline.

3.2 Astrometric Calibration

The astrometric calibration is realized in two steps. Firstly, the pipeline will work out a linear solution assuming the image has no distortion, based on the information stored in image headers, including the telescope pointing coordinates, the rotation angle and the pixel scale.

For further corrections, the pipeline employs a package named Software for Calibrating AstroMetry and Photometry (SCAMP, Bertin 2006) to derive astrometric solutions. SCAMP cooperates with SExtractor (Bertin & Arnouts 1996) by matching SExtractor's output catalog with an online or local reference catalog. SCAMP is mature and robust software that is widely used in astrometric calibration. The pipeline calls SCAMP twice. For the first run, a loose criterion for cross-matching detected sources with reference sources is used to retain enough stars for calibration. For the second run of SCAMP, a strict criterion is used to obtain a precise solution based on previous results. Table 4 shows the major configuration parameters for SCAMP in the two calls. The configurations are the same for both Bok and NOWT, and in particular we find DISTORT_DEGREES = 3 is the most suitable configuration after a series of tests.

The Position and Proper Motion Extended (PPMX, Röser et al. 2008) catalog is adopted in our pipeline as the astrometric reference. PPMX contains about 18 million stars which are evenly distributed across the whole sky with accuracies of $\sim$0.02″ in both RA and Dec directions. Over 85% of PPMX stars have V magnitudes between 10.0 and 15.0 mag, which matches very well with the dynamic ranges of our SAGES survey. As the *Gaia* DR2 (Gaia Collaboration et al. 2018) has just been released, we will use it as the astrometric reference in the future.

SDSS and Pan-STARRS DR1 (PS1, Chambers et al. 2016) are both accurate in astrometric and flux calibrations. However, SDSS covers only part of the sky, so we cannot use it as a reference catalog to ensure uniformity of the correction. PS1 has an uncertainty lower than 0.005″ in both RA and Dec, but it does not provide proper motions, so we do not use it as an astrometric reference, but we use it as the flux reference in Section 3.4.

Besides calling SCAMP, another astrometric calibration method is developed to provide an astrometric solution. Both methods are used in the pipeline so that we can compare their results to make sure we have the correct solution.

Generally, the purpose of the astrometric calibration is to fit a transformation formula from image coordinates (x, y) to celestial coordinates (α, δ), and then apply the formula to obtain the coordinates of all detected objects. The transformation usually has linear functions if there are not significant image distortions. However, because both the 90Prime and NOWT camera are at prime focus with a fast focal ratio, and the field-of-views are both larger than 1 deg^2, image distortions cannot be ignored and should be corrected.

The first step is to convert the original pixel coordinates (x, y), with the origin at the left-bottom corner, to intermediate pixel coordinates (u, v) with the origin at the center of the image. Then (u, v) is converted to intermediate world coordinates (ξ, η) using parameters CDi_j in the image header. Finally, (ξ, η) is projected to the world coordinates (α, δ), depending on the projection type, and our pipeline adopts the type 'TAN'. To resolve the non-linear correlation between (ξ, η) and (α, δ), we use the Simple Imaging Polynomial (SIP, Shupe et al. 2005) convention to represent image distortion. SIP adds

Table 4 The Major Configuration Parameters for SCAMP

Keyword	Round 1	Round 2	Note
MATCH	Y	Y	Module match or not
MATCH_NMAX	0	0	Upper bound for cross match
PIXSCALE_MAXERR	2	1.5	Max error of pixel scale
POSANGLE_MAXERR	5.0	2.0	Max error of position angle (degrees)
POSITION_MAXERR	10.0	1.0	Max error of position (arcmin)
MATCH_RESOL	0	0	Matching resolution
MATCH_FLIPPED	N	N	Allow axis flipping in match or not
CROSSID_RADIUS	25.0	2.0	Cross identification radius (arcsec)
SOLVE_ASTROM	Y	Y	Solve astrometric solution or not
PROJECTION_TYPE	SAME	SAME	Projection type
DISTORT_DEGREES	3	3	Degrees of distortion polynomial

high-order correction polynomials f and g to u and v to express the distortion, as shown in Equation (1)

$$\begin{pmatrix} \xi \\ \eta \end{pmatrix} = CD \times \begin{pmatrix} u + f(u,v) \\ v + g(u,v) \end{pmatrix} . \quad (1)$$

To determine polynomials f and g, A_{pq} and B_{pq} are used as the coefficients of $u^p v^q$ as shown in Equation (2), in which N_A and N_B are the highest order to correct u and v, respectively. After comprehensive tests, we find $N_A = N_B = 3$ is appropriate for SAGES.

$$\begin{aligned} f(u,v) &= \textstyle\sum_{p,q} A_{pq} \cdot u^p v^q, \quad 2 \le p+q \le N_A \,, \\ g(u,v) &= \textstyle\sum_{p,q} B_{pq} \cdot u^p v^q, \quad 2 \le p+q \le N_B \,. \end{aligned} \quad (2)$$

To evaluate internal astrometric errors yielded by the SAGES pipeline, comparisons have been made for all the fields with multiple visits, either in the same band or in different bands, and we calculate the differences in coordinates between different visits. Figure 8 displays a typical internal astrometric error, in which we find that $\Delta\mathrm{RA} = 0.014'' \pm 0.145''$ and $\Delta\mathrm{Dec} = -0.002'' \pm 0.166''$.

We determine the external astrometric errors by computing the difference between the computed coordinates and matched coordinates from the reference catalog PPMX. Figure 9 shows a typical distribution of external astrometric calibration errors. The errors are reasonable, with marginal offsets and small standard deviations of $\sim 0.1''$ in both RA and Dec, as marked in the lower-left panel of Figure 9. In conclusion, the internal and external astrometric uncertainties in SAGES are $\sim 0.1''$ in both directions. It can be improved in the future when employing *Gaia* DR2 as a reference catalog.

3.3 Source Detection and Aperture Photometry

To detect sources and perform photometric measurements, the software SExtractor (SE, Bertin & Arnouts 1996) is used in the SAGES pipeline. We set the detection threshold to be 4, which ensures that most sources could be found and measured by SE. After a successful run, SE will determine the following information with uncertainties for each source: the central positions of each source in both CCD physical coordinates and celestial coordinates, the roundness and sharpness, and instrumental magnitudes included in given aperture size(s). It will produce photometric results using different methods, among which some are appropriate for point sources and others for extended sources. Following the procedures applied in other surveys like SDSS (York et al. 2000) and SkyMapper (Wolf et al. 2018), we use the SE output MAG_AUTO as our primary output, as this output is in general reliable for both point sources and extended sources. The major SE configuration parameters used by our pipeline are listed in Table 5.

Source detection and photometry are performed based on the CCD used for data acquisition, and a global aperture size is adopted for all the stars in one CCD. However, an optimum aperture size should be adopted for faint stars to achieve small photometric errors, and aperture correction must be applied accordingly. We follow the process described in Howell (1989) to make accurate corrections using the aperture growth-curve method.

3.4 Flux Calibration

To achieve the scientific goals of accurate determinations of stellar parameters, SAGES is required to yield pho-

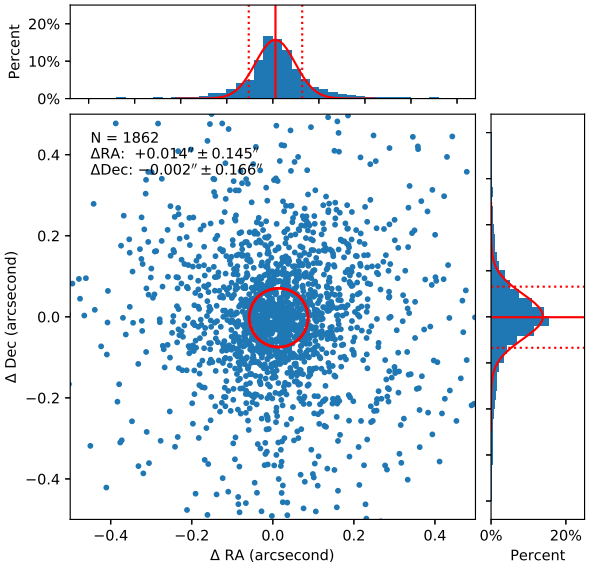

Fig. 8 Typical internal error of the astrometric results yielded by the SAGES pipeline, as compared to PPMX. The number of stars used for comparisons, the offsets and standard deviations are marked in the lower-left panel. In the top and right panels, the histograms of the differences in RA and Dec are plotted, respectively, with best-fit Gaussian-profile overplotted in *red*.

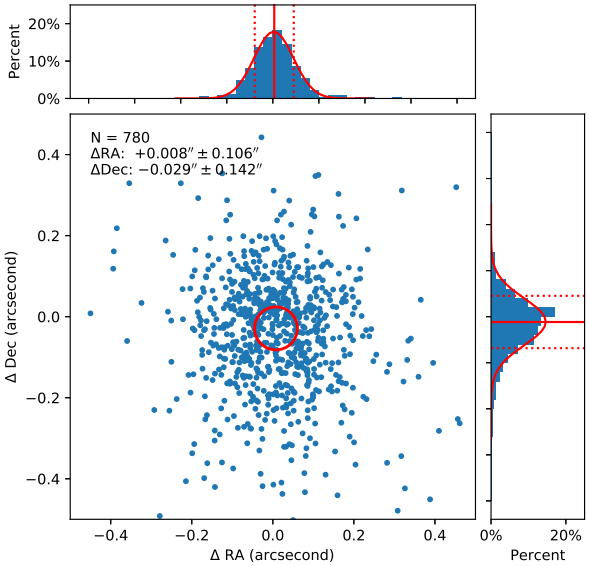

Fig. 9 The same as Fig. 8, but for typical external error.

Table 5 The Major Configuration Parameters for SE

Argument	Value	Note
DETECT_MINAREA	5	Minimum area of detection
DETECT_THRESH	4.0	Detection threshold
ANALYSIS_THRESH	4.0	Threshold used for analysis
PHOT_AUTOPARAMS	2.5, 3.5	Parameters to measure MAG_AUTO, Kron factor and minimum diameter
SATUR_LEVEL	45000.0	Saturation level before normalization
MAG_ZEROPOINT	25.0	Zeropoint of instrumental magnitude

tometry of stars brighter than 15 mag in V with accuracies better than 0.01 mag. To meet this requirement, high-precision flux calibration is essential, although it is extremely difficult to accomplish.

To correct for atmospheric extinction and transfer the instrumental magnitude to apparent magnitude for the SAGES survey, we use two methods of targeting standard stars or existing photometric surveys with well-calibrated photometry. In a photometric night, multiple observations targeting a set of standard stars are conducted at various airmasses, with which the atmospheric distinction curve can be derived. This curve will be applied to calibrate the apparent magnitude of stars observed during that night and any other photometric night. In Figure 10, we show the extinction curves derived in $u_{\rm SC}$ and $v_{\rm SAGE}$ on 2017 September 23 and 24 as examples.

For non-photometric nights, we have to rely on real-frame flux calibration by using the stars with high-precision magnitudes provided by previous surveys or catalogs. For SAGES, we use PS1 (Chambers et al. 2016) as the reference for flux calibration.

For the two filters $u_{\rm SC}$ and $v_{\rm SAGE}$ that have not been covered by PS1, we derived their magnitudes with a method trained from the g, r and i magnitudes. We select candidate stars from the spectral library by Pickles (1998). We convolve their spectrum with each filter transmission curve to determine the photometry in each band, with which we fit polynomial correlations between $u_{\rm SC}$ and $v_{\rm SAGE}$ with g, r and i as shown in Equation (3). With the derived correlation and the reddening maps given by Schlegel et al. (1998), for each PS1 star, its apparent that $u_{\rm SC}$ and $v_{\rm SAGE}$ magnitudes can be determined accordingly.

$$\begin{aligned} u_0 &= i_0 + 0.441 + 2.721(g-i)_0\,, \\ v_0 &= i_0 + 0.283 + 1.764(g-i)_0 + 0.181(g-i)_0^2\,. \end{aligned} \quad (3)$$

The derived magnitudes can only be used to estimate the observation depth and data quality. We are planning to perform calibration observations on several photometric nights, in order to produce a secondary flux reference catalog which can be used to calibrate all observation fields on all kinds of nights.

To evaluate the overall internal uncertainties of our image reduction, photometry and flux calibration, we compare the calibrated photometry of the same stars in different observations against photometry in Figure 11. The top and bottom panels are for the $u_{\rm SC}$ and $v_{\rm SAGE}$ bands, respectively. The x-axis is calibrated magnitudes and the y-axis is the difference between two exposures. The red curves show the 3σ loci by binning of 1.0 mag. We can find from the figure that the depths at SNR 5:1 are $u_{\rm SC}\sim$20 mag and $v_{\rm SAGE}\sim$19.5 mag and the depths at SNR 100:1 are $u_{\rm SC}\sim$16.5 mag and $v_{\rm SAGE}\sim$15.5 mag. These values of depths almost satisfy our goal. It is obvious that the internal photometric measurements need to be improved. We note that the $\sim$20% overlapping regions between adjacent fields will be very helpful to secure high-accuracy internal consistency in the entire survey area, and therefore the final uncertainties of flux calibrations should be similar or just slightly larger than those obtained with photometric stars observed on photometric nights.

4 TEST FIELD OF NGC 6791 AND ITS RESULT

4.1 Calibration Observations of NGC 6791

Wide-field imaging causes serious problems for accurate photometry due to field distortions, imperfect image quality near the edges of the field-of-view of the camera, and the non-uniformities of detectors and amplifiers in the large format of the mosaic camera. As for the case of fast focal ratio, the transmission curves of narrow- and medium-band filters might change from the center to the edge of the field-of-view.

To fully understand the situation in the instrument that we are using, and to make reliable field corrections, we performed a set of test observations of NGC 6791 on 2017 September 15. NGC 6791 is a well studied open cluster, centered at 19:20:50.7 +37:45:38.4 with an approximate diameter of 0.2 degrees (Warren & Cole 2009; Smolinski et al. 2011; Basu et al. 2011; Mészáros et al. 2013; Tofflemire et al. 2014; Hawkins et al. 2016). The angular size of NGC 6791 fits well into one amplifier of the 90Prime camera at the Bok telescope, and therefore it is appropriate to study the relative offsets between the 16 amplifiers of the 90Prime camera.

For each of the $u_{\rm SC}$ and $v_{\rm SAGE}$ filters, 16 exposures were taken at slightly different sky positions with each pointing toward NGC 6791 located at one of the 16 amplifiers. As a test, we used longer exposure times than regular survey observations, 100 s for $u_{\rm SC}$ and 40 s for $v_{\rm SAGE}$. These images were clear and the median FWHM of point sources detected in all images was $\sim 1.7''$. The coverage of our test observations is shown as the blue box in Figure 12; the 16 small crosses are the centers of each pointing and the $1.08^\circ \times 1.03^\circ$ green dotted box represents one example field pointing to the green cross.

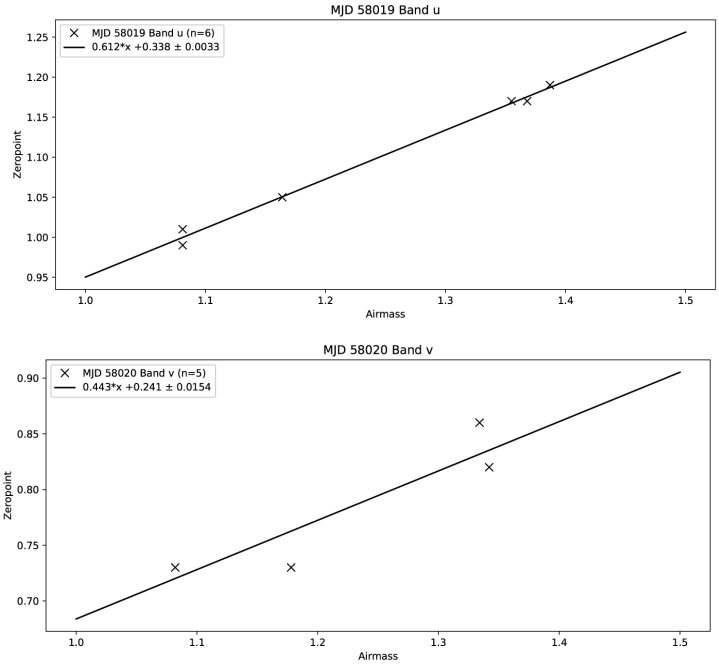

Fig. 10 The atmospheric extinction curves derived for $u_{\rm SC}$ and $v_{\rm SAGE}$ from data taken on 2017 Sep. 23 and 24, respectively at Kitt Peak.

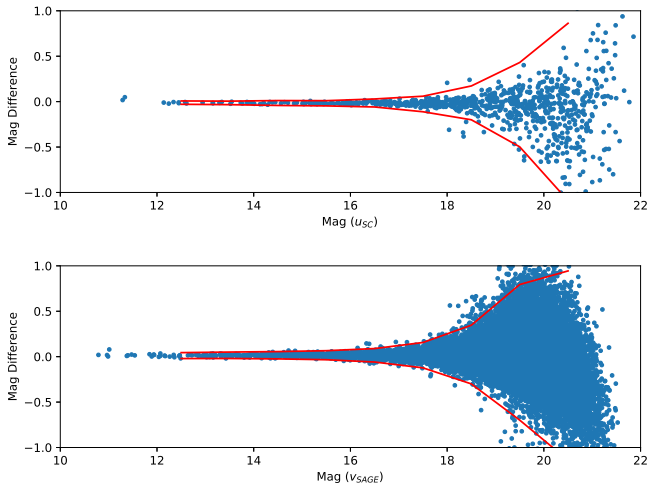

Fig. 11 Internal photometric uncertainties versus photometry for $u_{\rm SC}$ (*top*) and $v_{\rm SAGE}$ (*bottom*). The red curves show the 3σ loci.

The red stars signify the identified cluster members of NGC 6791 from works listed above.

4.2 Results of the Test Field

We have reduced and analyzed the test observation data, and have detected 109 472 objects in the $u_{\rm SC}$-band and 215 092 objects in the $v_{\rm SAGE}$-band with 4σ. The magnitude limits for single-exposure images are estimated by the APER magnitudes error at about 0.20 and 0.02 mag, which correspond to SNRs of 5 and 50, respectively. The median $u_{\rm SC}$- and $v_{\rm SAGE}$-band depths are 20.05 and 21.30 at 5σ and 17.16 and 18.37 at 50σ by the exposure times of 100 s and 40 s in $u_{\rm SC}$- and $v_{\rm SAGE}$-bands, respectively.

We plot the detected point sources in color-color diagrams in Figure 13 as blue dots. For comparison, synthetic colors of stars from the MILES stellar library (Falcón-Barroso et al. 2011), generated by convolving the transmission curves with the stellar spectrum, are

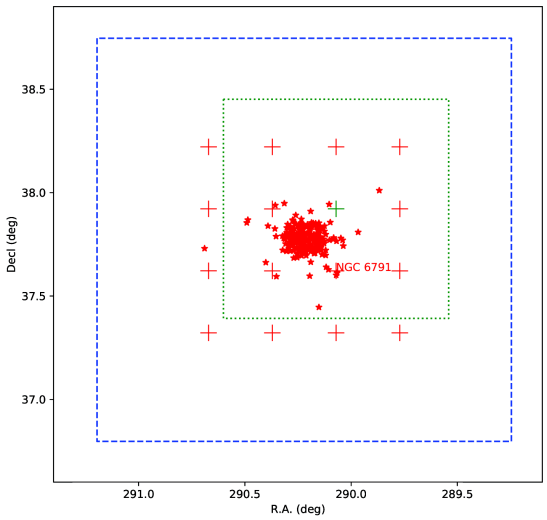

Fig. 12 The footprint of the test observations carried out around NGC 6791. The *blue dashed box* shows the coverage of the test observation, and the 16 *crosses* are the centers of each pointing, while the *green dotted box* indicates the field-of-view of the 90Prime centered at the *green cross*. The *red stars* mark the identified members of NGC 6791.

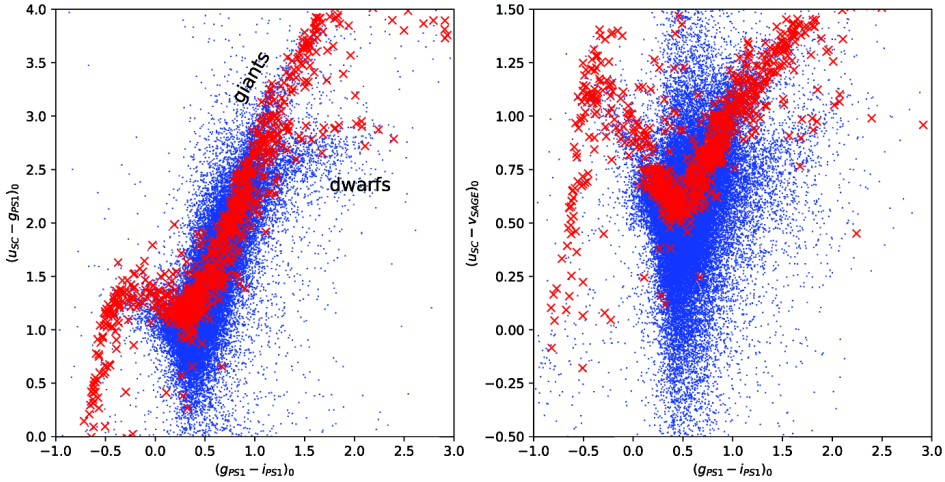

Fig. 13 The dereddened SAGE colors of stars (*blue dots*) detected in the test field around NGC 6791. The *red crosses* are synthetic colors of stars from the MILES stellar library.

overplotted in red. The measurements of g, r and i are taken from PS1. In the left panel, the bifurcation between cool dwarfs and cool giants is clear.

From the figure, it can be seen that the zero-points of the flux calibrations are correct. The experimental results are in good agreement with theoretical data. Meanwhile, the color calibrations are reliable.

5 SUMMARY

The SAGE photometric system is a specially-designed system that includes some existing filters and some newly-designed filters. This system is highly sensitive to stellar atmospheric parameters. We started the SAGE survey in 2015 and now about half of the observations have been acquired.

In this work, we describe the basic technical details of SAGES including instruments used for observations and the pipeline for image processing and data analysis. There is still quite some room to improve image reduction, astronomical calibration and flux calibrations. Around 2020, we expect to obtain high-quality photometry in eight colors of about 500 million stars and reliable measurements of their atmosphere parameters, with high-spatial resolution and a reliable extinction map. We

believe that SAGES will produce an important observational resource for investigations into stellar physics and the structure and evolution of the Milky Way Galaxy.

However, as our data reduction pipeline is not perfect, we are still working on improving it. The stripes in images need to be removed, and the photometric reference catalog of $u_{\rm SC}$ and $v_{\rm SAGE}$ is also being planned. Meanwhile, we are trying to perform flux evaluation with a higher precision.

Acknowledgements We thank Prof. Micheal Bessell and the SkyMapper team from the Research School of Astronomy and Astrophysics, Australian National University (RSAA, ANU) for their help and concern in the SAGE survey. Prof. Richard Green, Prof. Xiaohui Fan and other astronomers at the Steward Observatory, the University of Arizona, especially the mountain operation team, provided great help in observation and data reduction, and we thank them. We also received advice from the BATC group at NAOC. We appreciate help from all of them. This work is supported by the National Natural Science Foundation of China (Grant Nos. 11373003, 11673030 and U1631102), the National Key Basic Research Program of China (2015CB857002), and National Program on Key Research and Development Project (2016YFA0400804).

References

Árnadóttir, A. S., Feltzing, S., & Lundström, I. 2010, A&A, 521, A40

Basu, S., Grundahl, F., Stello, D., et al. 2011, ApJ, 729, L10

Bertin, E. 2006, in Astronomical Society of the Pacific Conference Series, 351, Astronomical Data Analysis Software and Systems XV, eds. C. Gabriel, C. Arviset, D. Ponz, & S. Enrique, 112

Bertin, E., & Arnouts, S. 1996, A&AS, 117, 393

Chambers, K. C., Magnier, E. A., Metcalfe, N., et al. 2016, arXiv:1612.05560

Crawford, D. L., Barnes, J. V., & Golson, J. C. 1970, AJ, 75, 624

Ehgamberdiev, S. A., Baijumanov, A. K., Ilyasov, S. P., et al. 2000, A&AS, 145, 293

Falcón-Barroso, J., Sánchez-Blázquez, P., Vazdekis, A., et al. 2011, A&A, 532, A95

Fan, Z., Zhao, G., Wang, W., et al. 2018, Progress in Astronomy, in press

Freyhammer, L. M., Andersen, M. I., Arentoft, T., Sterken, C., & Nørregaard, P. 2001, Experimental Astronomy, 12, 147

Fukugita, M., Ichikawa, T., Gunn, J. E., et al. 1996, AJ, 111, 1748

Gaia Collaboration, Brown, A. G. A., Vallenari, A., et al. 2018, arXiv:1804.09365

Hauck, B., & Mermilliod, M. 1998, A&AS, 129, 431

Hawkins, K., Masseron, T., Jofré, P., et al. 2016, A&A, 594, A43

Howell, S. B. 1989, PASP, 101, 616

Johnson, H. L., & Morgan, W. W. 1953, ApJ, 117, 313

Li, H., Aoki, W., Zhao, G., et al. 2015a, PASJ, 67, 84

Li, Y.-B., Luo, A.-L., Zhao, G., et al. 2015b, RAA (Research in Astronomy and Astrophysics), 15, 1364

Liu, J., Zhang, Y., Feng, G., & Bai, C. 2014, in IAU Symposium, 298, Setting the scene for Gaia and LAMOST, eds. S. Feltzing, G. Zhao, N. A. Walton, & P. Whitelock, 427

Mészáros, S., Holtzman, J., García Pérez, A. E., et al. 2013, AJ, 146, 133

Nordström, B., Andersen, J., Holmberg, J., et al. 2004, PASA, 21, 129

Pickles, A. J. 1998, PASP, 110, 863

Röser, S., Schilbach, E., Schwan, H., et al. 2008, A&A, 488, 401

Schlegel, D. J., Finkbeiner, D. P., & Davis, M. 1998, ApJ, 500, 525

Shi, Z. X., Comte, G., Luo, A. L., et al. 2014, A&A, 564, A89

Shupe, D. L., Moshir, M., Li, J., et al. 2005, in Astronomical Society of the Pacific Conference Series, 347, Astronomical Data Analysis Software and Systems XIV, eds. P. Shopbell, M. Britton, & R. Ebert, 491

Skrutskie, M. F., Cutri, R. M., Stiening, R., et al. 2006, AJ, 131, 1163

Smolinski, J. P., Lee, Y. S., Beers, T. C., et al. 2011, AJ, 141, 89

Strömgren, B. 1963, QJRAS, 4, 8

Strömgren, B. 1964, Astrophysica Norvegica, 9, 333

Tofflemire, B. M., Gosnell, N. M., Mathieu, R. D., & Platais, I. 2014, AJ, 148, 61

Wang, W., Zhao, G., Chen, Y., & Liu, Y. 2014, in IAU Symposium, 298, Setting the scene for Gaia and LAMOST, eds. S. Feltzing, G. Zhao, N. A. Walton, & P. Whitelock, 326

Warren, S. R., & Cole, A. A. 2009, MNRAS, 393, 272

Wolf, C., Onken, C. A., Luvaul, L. C., et al. 2018, PASA, 35, e010

York, D. G., Adelman, J., Anderson, Jr., J. E., et al. 2000, AJ, 120, 1579

Zhao, G., Zhao, Y.-H., Chu, Y.-Q., Jing, Y.-P., & Deng, L.-C. 2012, RAA (Research in Astronomy and Astrophysics), 12, 723

Zhao, J. K., Luo, A. L., Oswalt, T. D., & Zhao, G. 2013, AJ, 145, 169

Zou, H., Zhang, T., Zhou, Z., et al. 2017, AJ, 153, 276